JOURNAL OF GUIDANCE, CONTROL, AND DYNAMICS
Vol. 31, No. 5, September–October 2008

Lyapunov Vector Fields for Autonomous Unmanned Aircraft Flight Control

Dale A. Lawrence,* Eric W. Frew,† and William J. Pisano‡
University of Colorado, Boulder, Colorado 80309

DOI: 10.2514/1.34896

General techniques for constructing vector fields for unmanned aircraft guidance are provided that incorporate Lyapunov stability properties to produce simple, globally stable vector fields in three dimensions. Use of these fields to produce circular loiter pattern attractors is illustrated, along with a simple switching algorithm to enable following of arbitrary way point sequences. Alternatively, attractor shape variations are developed by warping the circular loiter, preserving global stability guarantees, and accurate path tracking. An example of this technique is provided that produces a racetrack loiter pattern, and three different variations in the warping technique are compared. Finally, tracking of the vector field is considered, using Lyapunov techniques to show global stability of heading and path position for several types of tracking control laws that are compatible with low cost unmanned aircraft avionics.

Nomenclature

a, b, l, m	=	control law parameters
$F(\bar{r})$	=	warping function mapping $\bar{r}$ to $\bar{q}$
$G(\bar{q})$	=	inverse warping function mapping $\bar{q}$ to $\bar{r}$
$H(\bar{r})$	=	weighting matrix
I	=	identity matrix
k	=	feedback inversion gain
L_i, J_i	=	time intervals
$\hat{n}$	=	unit normal to the loiter plane
$P(\dot{\bar{r}}, \dot{\bar{r}}_d)$	=	middle level feedback control law for vector field tracking
P_r	=	component of $P(\dot{\bar{r}}, \dot{\bar{r}}_d)$ parallel to $\dot{\bar{r}}$
$P_\perp$	=	component of $P(\dot{\bar{r}}, \dot{\bar{r}}_d)$ orthogonal to $\dot{\bar{r}}$
$\bar{q}$	=	UA position vector in parametric space
$\tilde{q}$	=	feedback inversion estimate for $\bar{q}$
R	=	bound on $\dot{\bar{r}}$
r	=	magnitude of UA position vector
$\bar{r}$	=	UA position vector relative to an inertial reference frame
$\ddot{\bar{r}}$	=	UA inertial acceleration vector
$\dot{\bar{r}}$	=	UA inertial velocity vector
$\tilde{r}$	=	feedback inversion estimate for $\bar{r}$
$\dot{\bar{r}}_d$	=	vehicle velocity vector produced by the Lyapunov vector field
$\ddot{\bar{r}}_d$	=	desired acceleration from the Lyapunov vector field
r_n	=	UA position component normal to loiter plane
$\bar{r}_t$	=	UA position component in the loiter plane
$S(\bar{r})$	=	circulation vector field component
(u, v, w)	=	coordinates of $\bar{q}$
$V_F(\bar{r})$	=	Lyapunov function defining the Lyapunov guidance vector field
$\dot{V}_F(\bar{r})$	=	time derivative of the Lyapunov function along the vector field
V_g	=	feedback inversion Lyapunov function
V_T	=	tracking Lyapunov function
$V_W(\bar{r})$	=	warped Lyapunov function
v	=	vector field magnitude (desired speed)
(x, y, z)	=	inertial frame coordinates of $\bar{r}$
(x_o, y_o, z_o)	=	loiter circle center
$\hat{z}$	=	downward-pointing unit vector
$\alpha(\bar{r})$	=	vector field normalizer
β	=	tracking gain
$\Gamma(\bar{r})$	=	weighting matrix
γ	=	relative circulation vs contraction weighting factor
θ	=	vector field parameter vector
$\lambda_{\min}\{\,\}$	=	minimum eigenvalue
ρ	=	loiter circle radius
χ	=	UA course angle
χ_d	=	desired course angle from the vector field
$\bar{\omega}$	=	course turning rate
$\langle\,\rangle$	=	$\text{mod}(-\pi, \pi]$

Presented as Paper 6317 at the Guidance, Navigation, and Control Conference, Hilton Head, SC, 20–23 August 2007; received 1 October 2007; revision received 31 January 2008; accepted for publication 1 February 2008. Copyright © 2008 by the American Institute of Aeronautics and Astronautics, Inc. All rights reserved. Copies of this paper may be made for personal or internal use, on condition that the copier pay the $10.00 per-copy fee to the Copyright Clearance Center, Inc., 222 Rosewood Drive, Danvers, MA 01923; include the code 0731-5090/08 $10.00 in correspondence with the CCC.

*Associate Professor, Aerospace Engineering Sciences, 429 UCB. Senior Member AIAA.

†Assistant Professor, Aerospace Engineering Sciences, 429 UCB. Member AIAA.

‡Ph.D. Candidate, Aerospace Engineering Sciences, 429 UCB. Student Member AIAA.

I. Introduction

AUTONOMY is essential for many unmanned aircraft (UA) applications. Remote piloting is not suitable for missions that are long in duration, have unreliable or delayed communication links, involve large numbers of vehicles, or require real-time data-driven cooperation between vehicles. At the same time, it is necessary that autonomous flight control be reliable, and in many current and envisioned applications, simple enough to implement in small flight computers found on low-cost vehicles.

Control over vehicle position is the ultimate objective of autonomous flight control, requiring sufficiently accurate measurements of position for the application at hand. The application also determines the type of position control that is needed. In midair refueling, formation flying, and target interception, relative position between UA and target is the critical measurement, and control must achieve sufficiently fast reduction of position error to the desired position offset (which may be zero). This is a *target tracking* type of flight control. In coordinated attack or rendezvous missions, particular georeferenced positions at particular times are needed, generating a *trajectory tracking* type of flight control. *Path tracking* occurs in applications such as border patrol, convoy protection, and air traffic holding patterns, where particular locations on a path at particular times are not important, as long as the vehicle converges to a georeferenced path and stays on it. *Waypoint following* requires the vehicle to fly over particular geolocations, usually in a specific order,

but the specific path between these locations is not constrained, nor is the time of overflight. Even less constrained are applications in *area* or *volume sampling*, where vehicle position is only constrained to be in the general vicinity of a particular location, for example, in a thunderstorm, where specific paths are not needed, and may be impossible to track anyway.

Clearly, highly constrained approaches can be used to satisfy less constrained applications. For example, path tracking can be achieved by defining a virtual target vehicle to track on the desired path [1–3] or by defining a specific trajectory to track that covers the desired path. However, these additional constraints may prevent a full utilization of freedom in the application to address other objectives and may present extraneous complications in trajectory planning.

The above control approaches can be described as explicit methods, where a particular positioning goal is defined a priori (volume/area, waypoint, path, trajectory, target), and control is designed to achieve that goal. Other approaches have appeared that can be described as implicit methods (also referred to as emergent behavior), in which the motion goal is not specified explicitly. Instead, motion results from particular control laws or agent behaviors on each vehicle, and behavior emerges [4–6] from the interaction of the control law with the environment or other vehicles.

This paper takes an explicit approach to autonomous flight control for applications in path tracking, waypoint following, and area/volume sampling. Reliability and simplicity motivate the development of a hierarchical control approach based on a vector field for vehicle guidance that provides an easy to implement control law relating vehicle position to desired velocity, and has provable global stability properties to limit cycle behavior. Lower levels in the hierarchy are then designed to ensure that the vehicle tracks this vector field. This provides a simple, yet highly capable basis for higher level algorithms that adjust the parameters of the vector fields to accomplish complex autonomous UA behaviors.

At the lowest level, control surfaces are used to produce aerodynamic moments to achieve stable dynamics and desired vehicle attitude. In turn, attitude relative to the airstream provides desired aerodynamic forces. These combine with gravity and propulsion forces to determine translational accelerations. Rigid body equations of motion and prevailing wind then determine the resulting velocity and position of the vehicle over time. See, for example, [7] for more detail. Here, it is presumed that the vehicle dynamics are sufficiently well known so that desired translational accelerations can be obtained, or well approximated, by low level flight control. The details of control at this level are vehicle specific and are not discussed in this paper.

The key layer in the hierarchical architecture described previously is the midlevel guidance controller. This layer is based on the Lyapunov vector field control concept which is a nonlinear cascade control approach [8], whereby a desired velocity vector field is specified that provides global attraction to a desired path and translational accelerations are used to align the UA velocity with this vector field. Given its simplicity and ease of implementation with limited computational resources, this notion of vector field control has received considerable recent attention for UA guidance in trajectory tracking [9], waypoint navigation [10], line following [11,12], stationary loitering [12], target observation [13], target tracking [14,15], and area/volume sampling [16].

Unlike these previous examples which have all used Lyapunov stability theory to *analyze* specific control laws (which have a corresponding induced vector field), we present a method for *designing* families of vector fields that are essentially globally asymptotically stable by construction. In particular, a general design approach is presented for constructing vector fields that have specified (nonzero) velocity everywhere, and that converge to closed, nonintersecting paths. Fixed wing aircraft must maintain airspeed to fly, so vector fields that converge to set points (equilibria) are not suitable. A detailed example is provided of the design of a vector field that converges to a circular (limit cycle) loiter pattern in 3-D. This design method is then extended to obtain other paths that are diffeomorphic to a circle, preserving global stability, and we show that several different warping variations are possible. Using these global constructions, the resulting vector fields are free of the ambiguities that arise in local methods, for example, in computing the closest point on the target path and the corresponding Serret–Frenet frame [13,14]. The global approach also obviates the construction of paths to destinations, such as waypoints, because the Lyapunov vector field provides well-behaved guidance to the destination from any initial location. Other work uses ad hoc vector field constructions [12–15,17] or vector fields derived from the particular physics of fluid flow [18], in contrast to the general vector field construction method provided here.

Furthermore, we analyze the resulting nonlinear cascade whereby translational acceleration is controlled by feeding forward desired acceleration with a term dependent on the error between the desired and actual velocity vectors. We demonstrate that this provides asymptotic path tracking under general conditions on the acceleration control law, illustrating this result with several examples that are compatible with micro air vehicle avionics capabilities. Of particular note, this vector field tracking approach does not require high gain control to achieve accurate path tracking.

The paper is organized as follows. Section II provides a general treatment of the Lyapunov vector field approach and illustrates this approach with a circular loiter example, which is similar to previous special cases [15,16,19–22]. It also discusses circular vector field switching to produce arbitrary waypoint following. Section III extends the circular attractor to other shapes via warping functions and discusses three different types of warping transformations. A racetrack loiter pattern is provided as an example. Section IV discusses acceleration control to produce vector field tracking, providing explicit techniques for the implementation of Lyapunov vector field guidance on small UAs.

II. Vector Field Construction

For vehicle guidance, we want to construct a vector field

$$\dot{\bar{r}}_d = h(\bar{r}, \theta(t)) \tag{1}$$

parameterized by a coefficient array θ, which may be a function of time. This provides a desired velocity vector $\dot{\bar{r}}_d$ at each vehicle position $\bar{r}$ (see Fig. 1) that can be used as a reference for control of vehicle acceleration. To understand the properties of the vector field itself, we assume in this section that the vehicle motion $\dot{\bar{r}}$ can be specified to equal any desired vector field $\dot{\bar{r}}_d$. (Section III discusses the tracking of a desired vector field using acceleration control.) Then Eq. (1) becomes a differential equation: $\dot{\bar{r}} = h(\bar{r}, \theta(t))$. If the vector field can be specified so that global behavior of solutions $\bar{r}(t)$ to the associated ordinary differential equation (ODE) can be specified to be simple and robust for all admissible values of θ, and the vehicle can track the reference vector field, then management of the vehicle can be accomplished at a higher hierarchical level by relatively infrequent manipulation of the parameters in θ. This promotes a high degree of autonomy in the vehicle and reduced communication bandwidth to centralized command and control systems.

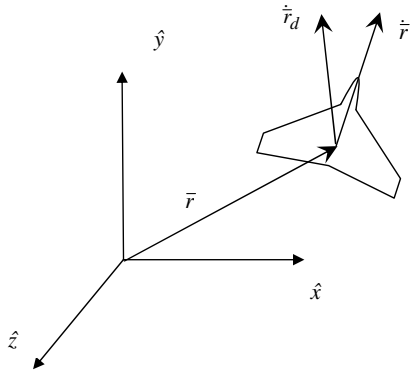

Fig. 1 UA inertial position and velocity, along with the desired velocity defined by the Lyapunov vector field.

Desired asymptotic behavior for $\bar{r}(t)$ is produced via an attractor, which consists of a path or equivalently a set of desired positions to which the vehicle should converge. In many other applications, this set could be a single equilibrium point, which implies an asymptotically fixed position (zero velocity). For fixed wing UAs, however, this is not possible because they must maintain airspeed to remain aloft. Here we are interested in attractors that allow asymptotic motion with nonzero velocity. Such attractors are continuous curves in configuration space and could take many forms, including chaotic "strange" attractors [23]. To provide well-understood vehicle behavior, however, we focus on the simplest of these attractors, that is, limit cycles. In this application, these are closed, non-self-intersecting curves C in $\mathbf{R}^3$ which contain no equilibrium points. The problem is then to construct a vector field $h(\bar{r}, \theta)$ that causes vehicle motion to be globally attracted to this set C.

We use the Lyapunov stability theory to construct a vector field, rather than to analyze a given vector field. In this approach, the desired attractor C is specified as a zero-level set of an otherwise positive scalar potential function $V_F(\bar{r})$. The specific conditions on $V_F(\bar{r})$ are as follows:

A1: $V_F(\bar{r})$ is positive definite on D with respect to C, that is, $V_F(\bar{r}) \geq 0$, $\forall\ \bar{r} \in D$, and $V_F(\bar{r}) = 0 \Rightarrow \bar{r} \in C$.

A2: $V_F(\bar{r})$ is radially unbounded, that is, $\bar{r} \to \infty$ implies that $V_F(\bar{r}) \to \infty$.

A3: $V_F(\bar{r})$ is continuously differentiable on an open domain $D \subseteq \Re^n$ and has no local extrema (other than on C) or inflection points, that is, $\partial V_F/\partial \bar{r} = \bar{0}$ implies that $V_F(\bar{r}) = 0$.

A4: $V_F(\bar{r})$ is not an explicit function of time, that is, the attractor C is fixed in time.

The following result gives a general class of vector fields derived from $V_F(\bar{r})$ that make C an attractor and also provides an explicit region of attraction.

Theorem 1: Let $\bar{r} \in D_a \subseteq D \subseteq \Re^n$, with D_a such that $a \geq V_F(\bar{r}) \geq 0$, $\forall\ \bar{r} \in D_a$, whose boundary is defined by $V_F(\bar{r}) = a$ and possibly $V_F(\bar{r}) = 0$. Let $\Gamma(\bar{r}, t)$: $D_a \times [0, \infty) \to \Re^{nxn}$ be continuous and uniformly positive definite on D_a uniformly in t, and continuous in t, and let $S(\bar{r}, t)$: $D_a \times [0, \infty) \to \Re^n$ be continuous on D_a, uniformly in t, and continuous in t, such that

$$\frac{\partial V_F}{\partial \bar{r}} S(\bar{r}) = 0, \quad \forall\ \bar{r} \in D_a \tag{2}$$

Then under conditions A1–A4, all integral curves of the vector field

$$\dot{\bar{r}} = h(\bar{r}, \theta(t)) = -\left[\frac{\partial V_F}{\partial \bar{r}} \Gamma(\bar{r}, t)\right]^T + S(\bar{r}, t) \tag{3}$$

beginning in D_a converge to the set C as $t \to \infty$.

Proof: For any $\bar{r} \in D_a$ the time derivative of $V_F(\bar{r})$ under A4 is given by

$$\dot{V}_F(\bar{r}) = \frac{\partial V_F}{\partial t} + \frac{\partial V_F}{\partial \bar{r}} \dot{\bar{r}} = \frac{\partial V_F}{\partial \bar{r}} h(\bar{r}, \theta(t)) \tag{4}$$

Then using Eq. (3),

$$\dot{V}_F(\bar{r}(t)) = -\left(\frac{\partial V_F}{\partial \bar{r}}\right) \Gamma(\bar{r}, t) \left(\frac{\partial V_F}{\partial \bar{r}}\right)^T \tag{5}$$

and since $\Gamma(\bar{r}, t)$ is positive definite, $\dot{V}_F(\bar{r}) \leq 0$. Hence, $V_F(\bar{r})$ converges, is bounded between a and 0, and D_a is positively invariant. Since $V_F(\bar{r})$ is a radially unbounded function (A2), D_a is compact. Then $\partial V_F/\partial \bar{r}$, $\Gamma(\bar{r}, t)$, and $S(\bar{r}, t)$ are uniformly continuous on D_a, uniformly in t, and so from Eq. (3), $\dot{\bar{r}}$ is bounded uniformly in t. Hence, $\bar{r}(t)$ is uniformly continuous in t, and from Eq. (5), $\dot{V}_F(\bar{r}(t))$ is also. By the Barbalat lemma [24], $\dot{V}_F(\bar{r}(t)) \to 0$. Since $\Gamma(\bar{r}, t)$ is uniformly positive definite, $\dot{V}_F(\bar{r}) \to 0$ implies that $\partial V_F/\partial \bar{r} \to \bar{0}$. By A3, this implies that $V_F(\bar{r}) \to 0$, and by A1, $\bar{r} \to C$. □

The first term in the vector field (3) is a contraction which produces a vector field component that is directed in opposition to the gradient of the potential function $V_F(\bar{r})$. When Γ is isotropic (a scaled identity matrix), this term is exactly opposite to the gradient of $V_F(\bar{r})$. A nonisotropic Γ allows a limited variation in this gradient-opposing direction, so that $V_F(\bar{r})$ remains monotone decreasing over time. The second term in Eq. (3) is a circulation term, which is always normal to the gradient of $V_F(\bar{r})$, and hence does not contribute to the change in $V_F(\bar{r})$ over time.

Observe that the function $S(\bar{r})$ should not be selected to be zero on the attractor C because in Eq. (3), $\partial V_F/\partial \bar{r} = \bar{0}$ requires that $\dot{\bar{r}} = S(\bar{r})$, and this would result in zero asymptotic vehicle velocity. For UA tracking control, it is desirable to choose $\Gamma(\bar{r}, t)$ and $S(\bar{r}, t)$ so that the vector field (3) is normalized to provide desired vehicle speed v at any point $\bar{r}$, that is,

$$|h(\bar{r}, \theta)| = \left| -\left[\frac{\partial V_F}{\partial \bar{r}} \Gamma(\bar{r}, t)\right]^T + S(\bar{r}, t) \right| = v(\bar{r}, t) \tag{6}$$

To preserve the constraints on $\partial V_F/\partial \bar{r}$, $\Gamma(\bar{r}, t)$, and $S(\bar{r}, t)$, v can be any positive constant, or any positive, continuous function of $\bar{r}$ and time that satisfies safe flight speed constraints on the vehicle, provided that $\Gamma(\bar{r})$ remains uniformly positive definite on compact domains D_a.

An example of functions $V_F(\bar{r})$, $\Gamma(\bar{r})$, and $S(\bar{r})$ that satisfy the conditions for Theorem 1 and produce a simple set C are as follows. This is similar to that originally provided [16]. Later work [12,15,19,20] has also used similar vector fields. Here, these vector fields are extended from 2-D to 3-D, enabling a complete treatment of lateral and vertical motions with the Lyapunov vector field approach. Also, the specific form of the vector field used here provides stronger attraction in the neighborhood of the loiter circle, compared to [15,16,20,22], resulting in better path tracking in the presence of disturbances. Let the coordinates of $\bar{r}$ be given by the difference between the vehicle location (x, y, z) and the center of a desired loiter circle attractor C at (x_o, y_o, z_o). Let the loiter circle lie in a plane normal to the unit vector $\hat{n}$, and let the desired in-plane radius of C be ρ. Define the normal and tangential (i.e., in-plane) components of $\bar{r}$ via projections onto $\hat{n}$ and the plane orthogonal to $\hat{n}$ via $\bar{r} = \hat{n}\hat{n}^T\bar{r} + (I - \hat{n}\hat{n}^T)\bar{r} = \bar{r}_n + \bar{r}_t$. Define corresponding scalar magnitudes $r_n = \hat{n}^T\bar{r}$ and $r_t = |\bar{r}_t|$, and define the Lyapunov function

$$V_F(\bar{r}) = \tfrac{1}{2} r_n^2 + \tfrac{1}{2}(r_t - \rho)^2 \tag{7}$$

Then with $\hat{r}_t = \bar{r}_t/|\bar{r}_t|$, $\bar{r}_t \neq \bar{0}$, we can derive

$$\frac{\partial V_F}{\partial \bar{r}} = r_n \hat{n}^T + (r_t - \rho)\hat{r}_t^T \tag{8}$$

The Lyapunov vector field (3) is then obtained with the definitions

$$\Gamma(\bar{r}, t) = \frac{1}{\alpha(\bar{r}, t)} I; \qquad S(\bar{r}, t) = \gamma(t) \frac{\hat{n} \times \bar{r}_t}{\alpha(\bar{r}, t)} \tag{9}$$

where $\gamma(t) > 0$ and the speed normalization $\alpha(\bar{r}, t)$ is given by

$$\alpha(\bar{r}, t) = \frac{1}{v(t)} (r_n^2 + (r_t - \rho)^2 + r_t^2 \gamma(t)^2)^{1/2} \tag{10}$$

Note that $V_F(\bar{r})$ is nonnegative and is zero only when the vehicle position $\bar{r}$ lies on the desired loiter circle C, so that $r_n = 0$ and $r_t = \rho$, satisfying (A1). Also, $\partial V_F/\partial \bar{r} \to 0$ implies $V_F(\bar{r}) \to 0$, and $\bar{r} \to \infty$ implies that $V_F(\bar{r}) \to \infty$, satisfying (A3) and (A2). If $\hat{n}$ is oriented vertically, the loiter circle is horizontal. Because Eqs. (8–10) produce Eq. (6), the vector field velocity is everywhere given by $v(t)$. Also, on C we have the vector field contraction term $(\partial V_F/\partial \bar{r})\Gamma(\bar{r}, t) = 0$ and from Eqs. (9) and (10), the vector field circulation term $|S(\bar{r}, t)| = v(t)$, providing the desired velocity on the loiter circle. The sign of $\gamma(t)$ in $S(\bar{r}, t)$ determines the direction of circulation on C. When $\bar{r}$ becomes large, the normalization (10) causes the circulation term $|S(\bar{r}, t)| \to 0$ and the contraction term $|(\partial V_F/\partial \bar{r})\Gamma(\bar{r}, t)| \to v(t)$. From Eq. (8), the vector field points toward the center of the loiter circle when far away and smoothly veers into a circular loiter as the radial distance converges to ρ. The magnitude of $\gamma(t)$ controls the relative strength of the circulation and

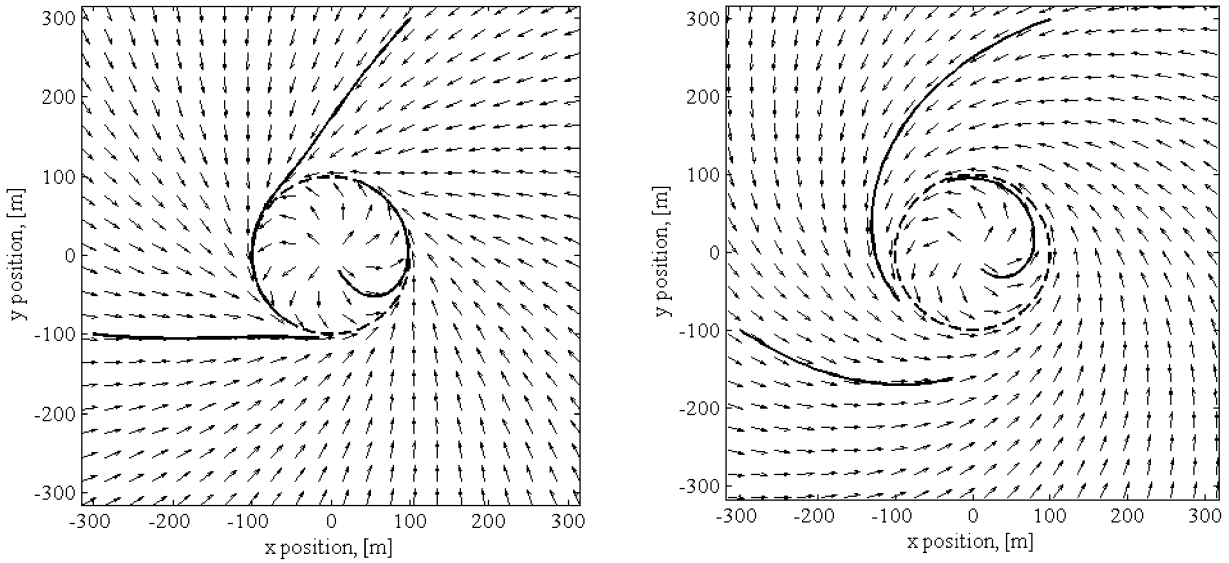

Fig. 2 Example vector field satisfying the assumptions for a globally attractive limit cycle, along with portions of integrated trajectories beginning at three different initial conditions. The left plot has a circulation parameter of $\gamma = 0.3$ and the right plot has $\gamma = 0.9$.

contraction terms, which modifies the abruptness of the transition from domination by contraction to domination by circulation. Likewise, a nonisotropic $\Gamma(\bar{r}, t)$ could be used to vary the strength of contraction normal to the circle relative to the contraction in the plane of the circle. Figure 2 shows this vector field for $(x_o, y_o, z_o) = (0, 0, 10)$ m, $\rho = 100$ m, and $v = 10$ m/s, along with some integrated trajectories beginning at various initial conditions. Two different circulation strengths are shown.

Applying Theorem 1 to Eq. (7) for $a < \rho^2/2$, the set D_a is a torus in $\Re^3$ centered on the loiter circle C [note $V_F(\bar{r}) = 0$ is not a boundary of D_a in this case, but lies inside the torus]. From Eq. (8), $\partial V_F/\partial \bar{r}$ is continuous everywhere except when $r_t = 0$ (where $\hat{r}_t$ is not defined), that is, except on the line normal to the loiter circle plane, passing through the center of the circle. Since D_a does not include this line, by construction, $\partial V_F/\partial \bar{r}$ is uniformly continuous on D_a. Also, $\Gamma(\bar{r}, t)$ and $S(\bar{r}, t)$ are uniformly continuous on $\Re^3$, uniformly in time, provided that $\gamma(t)$ and $v(t)$ are uniformly continuous, and $v(t)$ is positive and bounded away from zero. Then from Theorem 1 we have convergence of $\bar{r}$ to the loiter circle C beginning at any point in the torus D_a, $a < \rho^2/2$.

In fact, the region of attraction for C is *essentially global*, that is, it includes all initial conditions except those on a set of measure zero in $\Re^3$, that is, the line through the circle center identified previously. This can be shown by using Theorem 1 separately on two orthogonal, independent components of the vector field. Let $V_n = r_n^2/2$ and $V_t = (r_p - \rho)^2/2$, and identify components of $\bar{r}$ as $r_n \in \Re^1$ in the $\hat{n}$ direction and $\bar{r}_p \in \Re^2$ in the plane normal to $\hat{n}$. Note that $\bar{r}_t$ and $\bar{r}_p$ have different dimensions, but the same magnitude $r_p = r_t$ since $\bar{r}_t$ is zero in the $\hat{n}$ direction. Define the following regions (see Fig. 3) whose boundaries are defined by Lyapunov function values as required by Theorem 1:

$$D_{a1} = \{\bar{r}_p \in \Re^2 \mid 0 < \varepsilon \le r_p \le \rho\}$$
$$\text{where } 0 \le V_t \le a1 = (\rho - \varepsilon)^2/2$$

$$D_{a2} = \{\bar{r}_p \in \Re^2 \mid \rho \le r_p \le \delta\}$$
$$\text{where } 0 \le V_t \le a2 = (\delta - \rho)^2/2$$

$$D_{a3} = \{r_n \Re^1 \mid 0 \le |r_n| \le \sigma\} \quad \text{where } 0 \le V_n \le a3 = \sigma^2/2$$

From Eq. (9), the component of S is zero on D_{a3}, and $\Gamma = 1/\alpha(\bar{r}, t)$, hence Eq. (5) becomes $\dot{V}_n = -r_n^2/\alpha(\bar{r}, t)$. Similarly, on both D_{a1} and D_{a2}, S is orthogonal to $\bar{r}_p$ and $\Gamma = I_{2\times 2}/\alpha(\bar{r}, t)$, and Eq. (5) becomes $\dot{V}_t = -(r_p - \rho)^2/\alpha(\bar{r}, t)$. Since $\alpha(\bar{r}, t) > 0$, both V_n and V_t are bounded, and the sets D_{a1}, D_{a2}, and D_{a3} are positively invariant, r_n and $\bar{r}_p$ are bounded, and $1/\alpha(\bar{r}, t)$ is bounded away from zero. By Theorem 1, $r_n \to 0$ and $r_p \to \rho$, that is $\bar{r} \to C$. Since $\varepsilon > 0$ can be arbitrarily small and both $\delta > 0$ and $\sigma > 0$ can be arbitrarily large, all initial states except those on the line in $\bar{r} \in \Re^3$ defined by $r_p = 0$ converge to the attractor C.

This global behavior provides lower level behavior that is easy to build on for higher level control: essentially any initial state results in circular loitering flight centered at (x_o, y_o, z_o) with radius ρ and velocity v. It provides the UA with autonomous control which is simple to implement in an on-board microprocessor autopilot, as discussed in more detail in Sec. III. This globally attractive loiter circle behavior is specified through only six scalar parameters $\theta = (x_o, y_o, z_o, \rho, \gamma, v)$ and the three components of the normal vector $\hat{n}$. The parameters (γ, v) can be varied continuously, but the other parameters must be fixed in time for Theorem 1 to apply. However, these parameters can be switched occasionally, for example, to define a new attractor once the existing one is attained, resulting in an initial condition in the region of attraction of the new vector field, providing a variety of more complex guidance capabilities.

For example, the loiter circle approach can be used to construct robust waypoint navigation schemes, where the next waypoint is given as the loiter circle center, or as a point on the loiter circle so the vehicle flies directly over the waypoint. This approach is robust to waypoint generation timing: if the next waypoint is not available as the existing waypoint is approached, the vehicle will simply orbit the existing loiter center until the next one is available. No complex decision logic is needed to initiate turns. Also, the next waypoint vector field can be enabled based on proximity to the waypoint on the current target loiter circle, providing automatic sequencing of

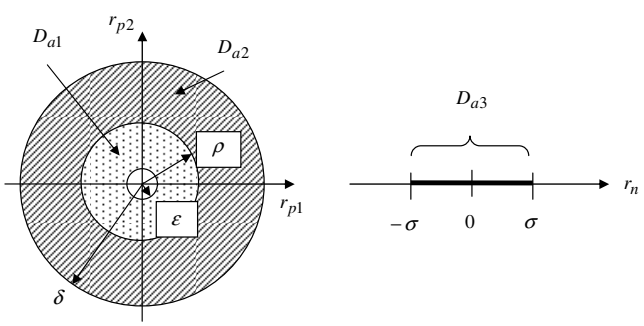

Fig. 3 Domains D_{a1}, D_{a2}, and D_{a3}.

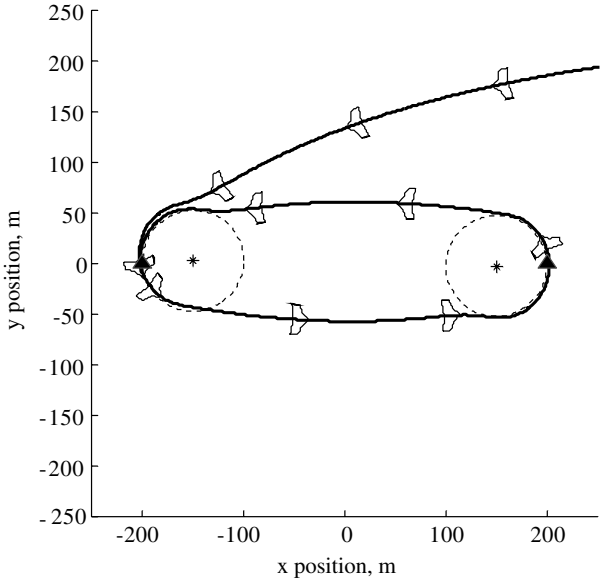

Fig. 4 Approximate racetrack loiter produced by switching between two circular loiter vector fields. The dashed circles represent the target loiter circles and the triangles are the two target waypoints that define the racetrack pattern.

waypoints to produce smooth transitions between waypoints. Although no formal theory is available, switching works well when the waypoints are separated by at least a loiter circle diameter, so that the next target loiter circle can be unambiguously defined, as explained in the example in Fig. 5.

Figure 4 shows a simulation of an aircraft following a "racetrack" pattern by switching between two loiter circle vector fields (star centers), anchored by two waypoints (triangles). The switch criterion is simple: the vehicle must have passed within a specified distance (10 m in this example) of the waypoint on the current loiter circle, and the vehicle heading must align within a specified error (11.5 deg in this case) to the vector field for the next waypoint. This provides a smooth transition between the two vector fields to produce an approximate racetrack loiter pattern. Switching based only on proximity to the loiter circle can produce undesirable flight paths, where the switch to the new vector field requires an abrupt direction change from the current heading. Although not as accurate as the racetrack obtained by warping a single circle loiter (cf. Sec. III), the switching approach is simple and flexible enough to enable on-board real-time changes in shape. In Fig. 4, only the two waypoints (triangles) and the desired loiter radii are required as inputs to the switched loiter circle autopilot. If the exact path is of less importance than reaching specific waypoints, then this simple vector field switching method should be considered.

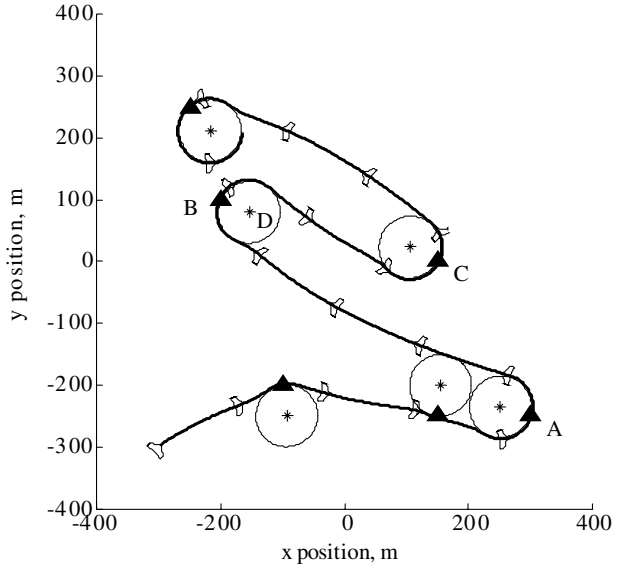

Fig. 5 An arbitrary waypoint (triangle) following an on-line planner and switching of circular vector fields (dashed target circles).

Extending this idea further, switching circular loiter vector fields can be used to follow arbitrary waypoint sequences that are produced by higher level task planning algorithms, for example, [25,26]. This enables more complex flight patterns, without the need for preprocessed route information. Figure 5 shows an example of an aircraft navigating a set of waypoints, where the algorithm is aware of only the most recent past waypoint A, the current target waypoint B (i.e., the waypoint defining the current vector field), and the next waypoint C. This information is used to produce a loiter circle passing through the current target waypoint, with center D bisecting the angle between lines joining the current waypoint and the previous and next waypoints. The lines AB and BC also determine the direction of circulation on the target loiter circle, that is, whether the next waypoint is to the right or left of the bearing to the current waypoint. As in Fig. 4, when the target waypoint is reached, switching to the next target loiter circle at the next waypoint is enabled and occurs when the aircraft heading and the next vector field are approximately aligned. This switching algorithm is simple enough to be run by the on-board autopilot, enabling upload of new waypoints in midflight. If the next waypoint is not available in time, the UA simply circles on the current loiter circle as shown at the last waypoint in Fig. 5.

Another application of loiter circles is in situ atmospheric sensing with large numbers [21] of small UAs. There, each vehicle is guided by its own loiter circle vector field, but data sensed in this process are used to autonomously modify the loiter circle location, for example, to cause vehicles to cluster in regions where high quality data are located. Here, a tilted loiter circle enables gradients of the atmospheric data to be estimated on each circuit, and this can be used to modify loiter circle location and diameter for desired clustering control. The robust, globally stable vector field behavior enables intervehicle coordination to be accomplished at higher levels in the control hierarchy and at lower rates of intercommunication.

The loiter circle approach has also been used for standoff tracking of ground targets [15,20], where range to the target optimizes the tradeoff between sensor accuracy and field of view, or where close approach to a hostile target is undesirable for stealth or safety reasons. Both this application and the atmospheric sensing application have time variation in the loiter circle parameter vector, that is, center location that can cause mistracking of the desired path, with errors proportional to the speed of parameter motion. In some cases, for example, [15], knowledge of the time variation can be used to recover asymptotic convergence, provided the parameter motion speed is smaller than the vehicle speed.

In other applications, globally attractive limit cycles may be desired, but with precise noncircular shapes. Modification of the shape of the limit cycle is discussed in the next section.

III. Shape Variations

A variety of alternative attractors can be obtained by a "warping" transformation of the basic circular loiter. This has the advantage of preserving the global stability properties of the vector field, but has some subtleties that can have unintended consequences. The most obvious approach is to morph the circle vector field using a change of coordinates. Suppose we map the "physical coordinates" $\bar{r} = (x, y, z)$ to "parametric coordinates" $\bar{q} = (u, v, w)$ by a diffeomorphism

$$\bar{q} = F(x, y, z) = F(\bar{r}) \tag{11}$$

so that the Jacobian $\partial F/\partial \bar{r}$ is nonsingular for all $\bar{r}$. Apply the Lyapunov vector field (3) in $\bar{q}$ coordinates, that is, with $\bar{q}$ in place of $\bar{r}$ to obtain $\dot{\bar{q}}$ and map this back by time differentiating (11):

$$\dot{\bar{q}} = \frac{\partial F}{\partial \bar{r}} \dot{\bar{r}} \tag{12}$$

This results in the vector field in the physical coordinates $\bar{r}$ in the form

$$\dot{\bar{r}} = h_1(\bar{r}) = \left[\frac{\partial F}{\partial \bar{r}}\right]^{-1} \dot{\bar{q}} = \left[\frac{\partial F}{\partial \bar{r}}\right]^{-1} \left[-\frac{\partial V_F}{\partial \bar{q}} \Gamma(\bar{q})\right]^T + \left[\frac{\partial F}{\partial \bar{r}}\right]^{-1} S(\bar{q}) \tag{13}$$

It is instructive to examine the evolution of the corresponding Lyapunov function $V_F(\bar{q}) = V_F(F(\bar{r})) = V_W(\bar{r})$:

$$\begin{aligned} \dot{V}_W(\bar{r}) &= \frac{\partial V_W}{\partial \bar{r}} \dot{\bar{r}} = \frac{\partial V_F}{\partial \bar{q}} \frac{\partial F}{\partial \bar{r}} \dot{\bar{r}} = \frac{\partial V_F}{\partial \bar{q}} \frac{\partial F}{\partial \bar{r}} \left[\frac{\partial F}{\partial \bar{r}}\right]^{-1} \dot{\bar{q}} \\ &= \frac{\partial V_F}{\partial \bar{q}} \frac{\partial F}{\partial \bar{r}} \left[\frac{\partial F}{\partial \bar{r}}\right]^{-1} \left(-\left[\frac{\partial V_F}{\partial \bar{q}} \Gamma(\bar{q})\right]^T + S(\bar{q})\right) \\ &= \frac{\partial V_F}{\partial \bar{q}} \left(-\Gamma(\bar{q}) \left[\frac{\partial V_F}{\partial \bar{q}}\right]^T + S(\bar{q})\right) = -\frac{\partial V_F}{\partial \bar{q}} \Gamma(\bar{q}) \left[\frac{\partial V_F}{\partial \bar{q}}\right]^T \end{aligned} \tag{14}$$

Compare this to the case that is obtained if we apply the approach of Eqs. (3) and (4), but in the $\bar{r}$ coordinates to directly obtain a Lyapunov vector field for $\dot{\bar{r}}$:

$$\dot{\bar{r}} = h_2(\bar{r}) = -\left[\frac{\partial V_W}{\partial \bar{r}} H(\bar{r})\right]^T + Q(\bar{r}); \qquad \frac{\partial V_W}{\partial \bar{r}} Q(\bar{r}) = 0 \tag{15}$$

If we choose

$$Q(\bar{r}) = \left[\frac{\partial F}{\partial \bar{r}}\right]^{-1} S(\bar{q}) \tag{16}$$

we have

$$\frac{\partial V_W}{\partial \bar{r}} Q(\bar{r}) = \frac{\partial V_F}{\partial \bar{q}} \frac{\partial F}{\partial \bar{r}} \left[\frac{\partial F}{\partial \bar{r}}\right]^{-1} S(F(\bar{r})) = \frac{\partial V_F}{\partial \bar{q}} S(\bar{q}) = 0 \tag{17}$$

If we also define the positive definite matrix $H(\bar{r})$ via

$$H(\bar{r}) = \left[\frac{\partial F}{\partial \bar{r}}\right]^{-1} \Gamma(F(\bar{r})) \frac{\partial F}{\partial \bar{r}} \tag{18}$$

then the vector field $\dot{\bar{r}}$ can be written as

$$\begin{aligned} \dot{\bar{r}} &= h_2(\bar{r}) = -\left[\frac{\partial V_F}{\partial \bar{q}} \frac{\partial F}{\partial \bar{r}} \left[\frac{\partial F}{\partial \bar{r}}\right]^{-1} \Gamma(\bar{q}) \frac{\partial F}{\partial \bar{r}}\right]^T + Q(\bar{r}) \\ &= \left[\frac{\partial F}{\partial \bar{r}}\right]^T \left[-\frac{\partial V_F}{\partial \bar{q}} \Gamma(\bar{q})\right]^T + \left[\frac{\partial F}{\partial \bar{r}}\right]^{-1} S(\bar{q}) \end{aligned} \tag{19}$$

This results in

$$\begin{aligned} \dot{V}_W(\bar{r}) &= \frac{\partial V_W}{\partial \bar{r}} \dot{\bar{r}} = \frac{\partial V_F}{\partial \bar{q}} \frac{\partial F}{\partial \bar{r}} \dot{\bar{r}} = -\frac{\partial V_F}{\partial \bar{q}} \frac{\partial F}{\partial \bar{r}} \left(\left[\frac{\partial V_F}{\partial \bar{q}} \frac{\partial F}{\partial \bar{r}} H(\bar{r})\right]^T\right) \\ &= -\frac{\partial V_F}{\partial \bar{q}} \left(\frac{\partial F}{\partial \bar{r}} \Gamma(\bar{q}) \left[\frac{\partial F}{\partial \bar{r}}\right]^T\right) \left[\frac{\partial V_F}{\partial \bar{q}}\right]^T \end{aligned} \tag{20}$$

Comparing Eq. (14) with Eq. (20) we see that an extra factor of $\partial F/\partial \bar{r}$ squared appears in the Lyapunov derivative in the second case. This shows that the evolution of Eq. (10) versus Eq. (15) will be different, although both forms result in the same asymptotic solutions since $\partial F/\partial \bar{r}$ is nonsingular. Note that when Γ is isotropic, so is H, and the second approach (19) uses the gradient of the warped Lyapunov function $V_W(\bar{r})$ in the contraction term, due to the factor $[\partial F/\partial \bar{r}]^T$. This makes the contraction portion of the vector field a covariant tensor [27]. In contrast, the use of $[\partial F/\partial \bar{r}]^{-1}$ in the corresponding place in Eq. (13) does not produce a contraction component in the negative gradient direction for $V_W(\bar{r})$. In this case, the contraction portion of the vector field is a contravariant tensor. The different contraction terms can change the direction of the vector field somewhat, at locations away from the attractor C, which can alter the trajectories toward the attractor. In both Eqs. (13) and (19), however, orthogonality of the circulation term to the gradient of $V_W(\bar{r})$ is preserved under warping, and so this term does not contribute to changes in $V_W(\bar{r})$ in either case.

A third alternative is to proceed as described previously, finding $\bar{q}$ from $\bar{r}$ using Eq. (11), and finding the vector field in $\bar{q}$ coordinates by using Eq. (3) with $\bar{q}$ in place of $\bar{r}$. However, to get the vector field $\dot{\bar{r}}$ simply use the vector field $\dot{\bar{q}}$, that is,

$$\dot{\bar{r}} = h_3(\bar{r}) = \dot{\bar{q}} = \left[-\frac{\partial V_F}{\partial \bar{q}} \Gamma(\bar{q})\right]^T + S(\bar{q}) \tag{21}$$

This is simpler to implement, but the global stability properties of the vector field in $\bar{q}$ coordinates do not necessarily translate to the same behavior in $\bar{r}$ coordinates in this case.

To illustrate the differences in the three previous warping approaches, we consider a warping function $\bar{q} = F(\bar{r})$ to produce a racetrack loiter pattern (Fig. 6), which has applications in convoy protection [15], and airstrip approach, holding, and landing patterns.

Although it may be possible in some applications to find an explicit function $\bar{q} = F(\bar{r})$ to provide the desired attractor shape, this may be difficult because the attractor is given by the inverse of this function applied to the circle in $\bar{q}$ coordinates. It may be more straightforward to construct the inverse function $\bar{r} = G(\bar{q})$ explicitly, so the image of the circle is easily compared to the desired attractor, and adjustments in $G(\bar{q})$ can be made to approximate the desired shape in $\bar{r}$ coordinates. We take this latter approach for the racetrack pattern, where $G(\bar{q})$ is given by

$$\bar{r} = \begin{bmatrix} x \\ y \\ z \end{bmatrix} = G(q) = \begin{bmatrix} g(u) \\ v \\ w \end{bmatrix} \quad \text{where } g(u) = u \frac{(|u| + b)}{(|u| + a)} \tag{22}$$

The parameters a and b are given by $a = \rho/20$ and $b = \rho(f - 1)$, where ρ is the radius of the unwarped circle, and $f > 1$ is the "stretch factor," which is approximately the ratio of the length of the racetrack over the diameter of the unwarped loiter circle. Note that only the x coordinate is warped in this example, but an arbitrary orientation of the racetrack could be specified by rotating coordinates after applying the stretch function along one direction as above. The Jacobian of F is given by

$$\frac{\partial F}{\partial \bar{r}} = \left[\frac{\partial G}{\partial \bar{q}}\right]^{-1} = \begin{bmatrix} \left(\frac{\mathrm{d}g}{\mathrm{d}u}\right)^{-1} & 0 & 0 \\ 0 & 1 & 0 \\ 0 & 0 & 1 \end{bmatrix} \tag{23}$$

$$\text{where } \frac{\mathrm{d}g}{\mathrm{d}u} = \frac{(|u| + a)^2 + a(b - a)}{(|u| + a)^2}$$

The function $g(u)$ is actually C^1, despite the $|u|$ terms, because derivatives of $|u|$ in $\mathrm{d}g/\mathrm{d}u$ are multiplied by u and $u\mathrm{d}|u|/\mathrm{d}u = |u|$ is continuous at 0. Note that if $f > 1$, then $\partial G/\partial \bar{q}$ is nonsingular for all $\bar{q}$, since $ab > 0$.

To use this warping function, we must find the parametric coordinate u for each position x. In this example, there is a closed form solution for $u = g^{-1}(x)$, given by noting that $\mathrm{sign}(u) = \mathrm{sign}(x)$ in Eq. (22) when $f > 1$ and applying the quadratic formula to solve

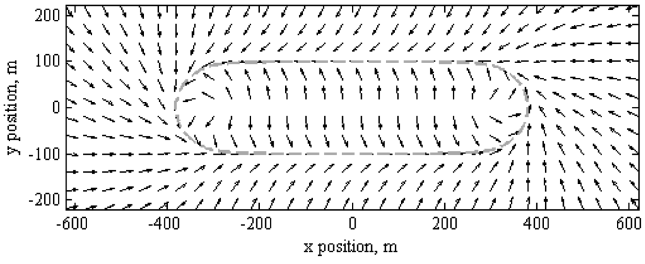

Fig. 6 Precise racetrack attractor achieved by warping the circular guidance vector field, using the covariant inverse mapping.

for u:

$$u = \text{sign}(x)\left[\frac{|x|-b}{2} + \sqrt{\left(\frac{|x|-b}{2}\right)^2 + a|x|}\right] \tag{24}$$

A more general approach is to compute F as the feedback inverse of G, as follows. For any *fixed* $\bar{r}$, let

$$\dot{\tilde{q}} = k\left[\frac{\partial G}{\partial \tilde{q}}\right]^{-1}(\bar{r} - \tilde{r})$$

where $\tilde{r} = G(\tilde{q})$, and $k > 0$. Then $\tilde{q} \to F(\bar{r})$, which can be seen from the Lyapunov function $V_g = (\bar{r} - \tilde{r})^T(\bar{r} - \tilde{r})$ whose time derivative is

$$\begin{aligned}\dot{V}_g &= 2(\bar{r} - \tilde{r})^T(-\dot{\tilde{r}}) = -2(\bar{r} - \tilde{r})^T \frac{\partial G}{\partial \tilde{q}}\dot{\tilde{q}} \\ &= -2k(\bar{r} - \tilde{r})^T \frac{\partial G}{\partial \tilde{q}}\left[\frac{\partial G}{\partial \tilde{q}}\right]^{-1}(\bar{r} - \tilde{r}) = -2k|\bar{r} - \tilde{r}|^2 \end{aligned} \tag{25}$$

Since $\dot{V}_g = -2kV_g$, the error $|\bar{r} - \tilde{r}|$ goes to zero at the exponential rate of e^{-kt}. When $\bar{r}$ is not fixed, the position $\tilde{q}$ generated by this algorithm will be an accurate estimate of the corresponding parametric location given by $F(\bar{r}) = G^{-1}(\bar{r})$, provided that the convergence rate of V_g is fast enough compared to the rate of change of the vehicle position $\bar{r}$. More precisely, when $\dot{\bar{r}}$ is nonzero, Eq. (25) becomes

$$\dot{V}_g = -2kV_g + 2(\bar{r} - \tilde{r})^T(\dot{\bar{r}}) \tag{26}$$

Using the standard solution to a first-order linear ODE with input $2(\bar{r} - \tilde{r})^T(\dot{\bar{r}})$

$$V_g(t) = e^{-2kt}V_g(0) + \int_0^t e^{-2k(t-\tau)}2(\bar{r} - \tilde{r})^T(\dot{\bar{r}})\,\mathrm{d}\tau$$

Hence by defining $\tilde{V}_g(t) = V_g(t) - e^{-2kt}V_g(0)$ and with $\dot{\bar{r}}$ bounded by R, we have

$$\tilde{V}_g(t) = \int_0^t e^{-2k(t-\tau)}2(\bar{r} - \tilde{r})^T(\dot{\bar{r}})\,\mathrm{d}\tau \le 2R\int_0^t e^{-2k(t-\tau)}|\bar{r} - \tilde{r}|\,\mathrm{d}\tau \tag{27}$$

At each time, either $|\bar{r} - \tilde{r}| < 1$, or $|\bar{r} - \tilde{r}| \ge 1$ in which case

$$|\bar{r} - \tilde{r}| \le |\bar{r} - \tilde{r}|^2 = V_g = \tilde{V}_g + e^{-2kt}V_g(0)$$

and so

$$\begin{aligned}\tilde{V}_g(t) &\le 2R\int_0^t e^{-2k(t-\tau)}(1 + e^{-2k\tau}V_g(0))\,\mathrm{d}\tau \\ &\quad + 2R\int_0^t e^{-2k(t-\tau)}\tilde{V}_g(\tau)\,\mathrm{d}\tau \\ &= \left(\frac{R}{k}(1 - e^{-2kt}) + 2RV_g(0)te^{-2kt}\right) \\ &\quad + 2R\int_0^t e^{-2k(t-\tau)}\tilde{V}_g(\tau)\,\mathrm{d}\tau \end{aligned} \tag{28}$$

This is of the form

$$\tilde{V}_g \le \lambda(t) + \phi(t)\int_0^t \mu(\tau)\tilde{V}_g(\tau)\,\mathrm{d}\tau$$

where

$$\lambda(t) = \left(\frac{R}{k}(1 - e^{-2kt}) + 2RV_g(0)te^{-2kt}\right) \ge 0$$

$\phi(t) = 2Re^{-2kt} \ge 0$, and $\mu(\tau) = e^{2k\tau}$. By the Bellman–Gronwall lemma [28] we have

$$\tilde{V}_g(t) \le \lambda(t) + 2R\int_0^t e^{2(R-k)(t-\tau)}\lambda(\tau)\,\mathrm{d}\tau \tag{29}$$

Since $\lambda(t)$ is bounded, when $k > R$ so is $\tilde{V}_g$, and since $\tilde{V}_g \to V_g$, so is V_g. Carrying out the integration for the three terms of $\lambda(\tau)$ in Eq. (29), we also find that V_g is ultimately bounded as $t \to \infty$ by

$$V_g \le \frac{R}{k} + \frac{2R^2}{k(k-R)} \tag{30}$$

Hence the asymptotic tracking error $V_g = (\bar{r} - \tilde{r})^T(\bar{r} - \tilde{r})$ can be made as small as desired by choosing the feedback inversion gain k sufficiently large compared to the vehicle velocity bound R. Because this feedback inversion is an algorithm (not a feedback control of a physical system), a robust way to achieve fast convergence rates is to use moderate gains k in a discrete time update for $\tilde{q}$, but iterate the algorithm many times before updating each new vector field calculation.

The vector field found through this method of feedback inverse warping is shown in Fig. 6. The solid line is the streamline resulting from integrating the warped vector field, using the contravariant unwarping method (13).

The three different unwarping methods (13), (19), and (21) are compared in Fig. 7. For this shape, the resulting vector field has subtle differences in vehicle motion toward the racetrack attractor, which may cause one of these methods to be preferred, depending on the application. In particular, the covariant (19) and unity (13) methods are most similar overall, and the contravariant (21) method has undesirable small radius turns. Also, the unity method has poor accuracy on the attractor, while the other two converge precisely. Global stability is guaranteed for the covariant and contravariant warping methods, but not for the unity unwarping (21). It is important to note that the various unwarping transformations can significantly affect the relative sizes of the circulation and contraction portions of the vector field, and separate renormalization of these components is required to preserve the relative sizes of these terms. Otherwise, the resulting vector field in physical coordinates can be highly distorted and produce unexpected results.

IV. Vector Field Tracking

A. Vector Field Convergence

To control a vehicle to track the Lyapunov vector field $\dot{\bar{r}}_d$ using applied accelerations, consider the following control law:

$$\ddot{\bar{r}} = -P(\dot{\bar{r}}, \dot{\bar{r}}_d) + \ddot{\bar{r}}_d = -P(\dot{\bar{r}}, h(\bar{r})) + \ddot{\bar{r}}_d \tag{31}$$

where $\dot{\bar{r}}_d = h(\bar{r}, t)$ is given by, for example, Eqs. (3) and (13) or Eq. (19), and hence

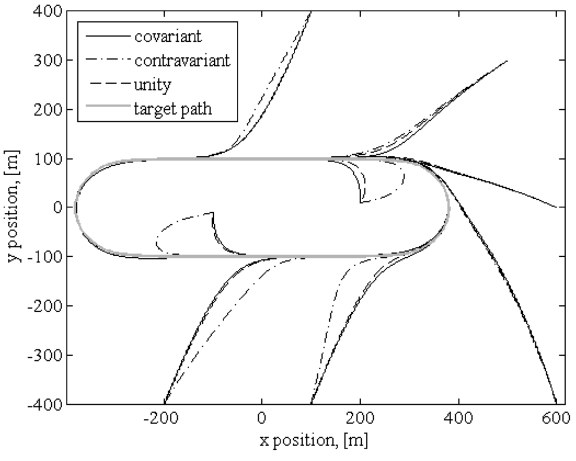

Fig. 7 Comparison of three inverse mapping methods.

$$\ddot{\bar{r}}_d = \frac{\partial h}{\partial \bar{r}}\dot{\bar{r}} + \frac{\partial h}{\partial t}$$

We assume the following:

A5: The function $(\dot{\bar{r}} - h(\bar{r}))^T P(\dot{\bar{r}}, h(\bar{r}))$ is a uniformly continuous function of $(\dot{\bar{r}} - h(\bar{r}))$, and positive semidefinite in the sense that $(\dot{\bar{r}} - h(\bar{r}))^T P(\dot{\bar{r}}, h(\bar{r})) \geq 0$ and $(\dot{\bar{r}} - h(\bar{r}))^T P(\dot{\bar{r}}, h(\bar{r})) = 0$ implies that $P(\dot{\bar{r}}, h(\bar{r})) = 0$, and $P(\dot{\bar{r}}, h(\bar{r}))$ is bounded whenever $\dot{\bar{r}}$ and $h(\bar{r})$ are bounded.

A6: The vector field $h(\bar{r}, t)$ is bounded, for example, by the normalization in Eq. (6).

Theorem 2: Under A5 and A6, the control law (31) produces $P(\dot{\bar{r}}, h(\bar{r})) \to 0$.

Proof: Consider the following vector field tracking Lyapunov function:

$$V_T = (\dot{\bar{r}} - h(\bar{r}))^T (\dot{\bar{r}} - h(\bar{r})) \tag{32}$$

The time derivative of this is

$$\begin{aligned}\dot{V}_T &= 2(\dot{\bar{r}} - h(\bar{r}, t))^T \left(\frac{\partial(\dot{\bar{r}} - h(\bar{r}, t))}{\partial \bar{r}}\dot{\bar{r}} + \frac{\partial(\dot{\bar{r}} - h(\bar{r}, t))}{\partial \dot{\bar{r}}}\ddot{\bar{r}} \right. \\ &\left. + \frac{\partial(\dot{\bar{r}} - h(\bar{r}, t))}{\partial t} \right) = 2(\dot{\bar{r}} - h(\bar{r}, t))^T \left(-\frac{\partial h}{\partial \bar{r}}\dot{\bar{r}} - P(\dot{\bar{r}}, h(\bar{r}, t)) \right. \\ &\left. + \frac{\partial h}{\partial \bar{r}}\dot{\bar{r}} + \frac{\partial h}{\partial t} - \frac{\partial h}{\partial t} \right) = -2(\dot{\bar{r}} - h(\bar{r}, t))^T P(\dot{\bar{r}}, h(\bar{r}, t)) \end{aligned} \tag{33}$$

which uses Eq. (31) for $\ddot{\bar{r}}$ and the expression after Eq. (31) for $\ddot{\bar{r}}_d$. Since P is positive semidefinite, $\dot{V}_T \leq 0$ and V_T converges. Hence, V_T and $(\dot{\bar{r}} - h(\bar{r}))$ are bounded. From A6, $\dot{\bar{r}}$ is bounded. Hence P in Eq. (31) is bounded. Then $\frac{\mathrm{d}}{\mathrm{d}t}(\dot{\bar{r}} - h(\bar{r}))$ is bounded and $(\dot{\bar{r}} - h(\bar{r}))$ is uniformly continuous. Then $\dot{V}_T(t)$ in Eq. (33) is uniformly continuous and by Barbalat, $\dot{V}_T \to 0$. Hence, $P(\dot{\bar{r}}, h(\bar{r})) \to 0$. □

This result does not immediately imply that $\dot{\bar{r}} - h(\bar{r}) \to 0$. P must be selected carefully to obtain this result from the results of Theorem 2. A simple choice for the control law P is given by $P(\dot{\bar{r}}, h(\bar{r})) = \beta(\dot{\bar{r}} - h(\bar{r}))$ with $\beta > 0$. In this case, $\dot{V}_T = -2\beta V_T$ and V_T and $\dot{\bar{r}} - h(\bar{r})$ converge exponentially to zero, achieving asymptotic tracking of the vector field velocity. Unfortunately, if $\dot{\bar{r}}$ is initialized near the opposite direction from $h(\bar{r})$, then the vehicle speed $|\dot{\bar{r}}|$ can pass very close to zero on its way to converge to $h(\bar{r})$. Also, no acceleration limits are imposed with this approach (e.g., to limit turn rate, or climb rate).

One way to incorporate limits is to use a P in the form

$$P(\dot{\bar{r}}, h(\bar{r})) = P_\perp \cdot (\dot{\bar{r}} - h(\bar{r})) + P_r \cdot (\dot{\bar{r}} - h(\bar{r}))$$

where

$$P_\perp = \frac{m}{m + |\dot{\bar{r}} - h(\bar{r})|}\left(I - \frac{\dot{\bar{r}}\dot{\bar{r}}^T}{|\dot{\bar{r}}|^2} \right); \qquad P_r = \frac{l}{l + |\dot{\bar{r}} - h(\bar{r})|} \cdot \frac{\dot{\bar{r}}\dot{\bar{r}}^T}{|\dot{\bar{r}}|^2} \tag{34}$$

are scaled projections onto the subspaces orthogonal to and parallel to $\dot{\bar{r}}$, respectively. The scaling limits the size of the projection to limit turn rate/vertical acceleration (by m) and to limit the rate of change in speed (by l). When $m > 0$, $l > 0$, $P(\dot{\bar{r}}, h(\bar{r})) \to 0$ implies that $\dot{\bar{r}} - h(\bar{r})$ converges to zero. By making l small compared to m, this control law encourages $\dot{\bar{r}}$ to converge to $h(\bar{r})$ by turning or climbing instead of changing speed.

Another special case of P corresponds to a common approach in tracking 2-D vector fields, using the so-called kinematic model of airplane flight [12]. Let χ be the instantaneous course angle of the vehicle, which is the angle between the north pointing axis and the horizontal component of $\dot{\bar{r}}$, measured clockwise. Then the angular velocity of the horizontal component of $\dot{\bar{r}}$ (turning rate) is given by $\bar{\omega} = \dot{\chi}\hat{z}$, where $\hat{z}$ is the downward-pointing vertical unit vector. Similarly, let χ_d be the desired course angle derived from the vector field $\dot{\bar{r}}_d = h(\bar{r})$, and let $\bar{\omega}_d = \dot{\chi}_d\hat{z}$ be the corresponding turning rate of $\dot{\bar{r}}_d$. Then the control law

$$\dot{\chi} = k\langle \chi_d - \chi \rangle + \dot{\chi}_d \tag{35}$$

for positive gain k and $\langle \chi_d - \chi \rangle = (\chi_d - \chi)(-\pi, \pi]$ (the so-called "wrapped" version of the course angle error) can be written as $\bar{\omega} = k\langle \chi_d - \chi \rangle\hat{z} + \bar{\omega}_d$. Assuming the vehicle velocity has the same (constant) magnitude as the vector field, and these are both horizontal, we have $\ddot{\bar{r}}_d = \bar{\omega}_d \times \dot{\bar{r}}_d = \bar{\omega}_d \times \dot{\bar{r}}$. Setting $\ddot{\bar{r}} = \bar{\omega} \times \dot{\bar{r}}$ produces the acceleration control law

$$\ddot{\bar{r}} = k\langle \chi_d - \chi \rangle\hat{z} \times \dot{\bar{r}} + \ddot{\bar{r}}_d \tag{36}$$

from which $P(\dot{\bar{r}}, \dot{\bar{r}}_d)$ in Eq. (31) can be recognized as $-k\langle \chi_d - \chi \rangle\hat{z} \times \dot{\bar{r}}$. Note that this control law does not change the magnitude of the vehicle velocity, since

$$\frac{\mathrm{d}}{\mathrm{d}t}|\dot{\bar{r}}|^2 = 2\dot{\bar{r}}^T\ddot{\bar{r}} = 2\dot{\bar{r}}^T(\bar{\omega} \times \dot{\bar{r}}) \equiv 0 \tag{37}$$

and $\dot{\bar{r}}$ remains horizontal if $\dot{\bar{r}}_d$ does, since $\hat{z}^T\ddot{\bar{r}} = \hat{z}^T(k\langle \chi_d - \chi \rangle\hat{z} \times \dot{\bar{r}} + \ddot{\bar{r}}_d) \equiv 0$. Checking the conditions on $P(\dot{\bar{r}}, \dot{\bar{r}}_d)$ for stability, observe that the positive semidefinite part of A5 is satisfied:

$$\begin{aligned}(\dot{\bar{r}} - h(\bar{r}))^T P(\dot{\bar{r}}, h(\bar{r})) &= -k\langle \chi_d - \chi \rangle (\dot{\bar{r}} - h(\bar{r}))^T(\hat{z} \times \dot{\bar{r}}) \\ &= k\langle \chi_d - \chi \rangle h(\bar{r})^T(\hat{z} \times \dot{\bar{r}}) = k\langle \chi_d - \chi \rangle (\dot{\bar{r}} \times h(\bar{r}))^T\hat{z} \\ &= k|h(\bar{r})||\dot{\bar{r}}|\langle \chi_d - \chi \rangle \sin\langle \chi_d - \chi \rangle \geq 0 \quad \forall\ \chi_d - \chi \end{aligned} \tag{38}$$

Consider any initial condition where $|\chi_d - \chi| \leq w < \pi$. From Eq. (33) $|\dot{\bar{r}} - \dot{\bar{r}}_d|$ is nonincreasing, hence $|\chi_d - \chi| \leq w < \pi$ remains true, and $P(\dot{\bar{r}}, \dot{\bar{r}}_d)$ is a uniformly continuous function of $(\dot{\bar{r}} - h(\bar{r}))$ on this domain, satisfying A5. Now $(\dot{\bar{r}} - h(\bar{r}))^T P(\dot{\bar{r}}, h(\bar{r})) = 0$ implies either $\chi_d - \chi = 0$, or $\chi_d - \chi = \pi$, or $\dot{\bar{r}} = 0$, or $\dot{\bar{r}}_d = h(\bar{r}) = 0$. The last two alternatives are prevented by the constant (nonzero) velocity produced by Eq. (37) and the nonzero vector field. The case $\chi_d - \chi = \pi$ cannot occur, as just argued. Then by the LaSalle invariance principle, Eq. (33) shows that $\chi_d - \chi \to 0$. [The vector field h is time invariant in this case, making Eq. (35) an autonomous system, and so the LaSalle invariance principle can be applied.] Given that $\dot{\bar{r}}$ and $\dot{\bar{r}}_d$ are horizontal, and have the same magnitude, we also have $\dot{\bar{r}} \to \dot{\bar{r}}_d$.

It is interesting to note that the work of [12] takes a sliding mode approach that replaces the natural tracking dynamics and the vector field turning rates in Eq. (36) with a high gain saturation function of the vector field-to-vehicle course error. The approach offered here [stemming from Eq. (31)] avoids practical problems with chattering and control saturation by feeding forward the vector field turn rate, achieving accurate tracking with relatively low gains on course errors. Similarly, wind disturbances can be addressed as in [12] using high gains, or alternatively by using low gains together with additional estimated wind feedforward terms in Eq. (31), as in [15,20].

B. Attractor Convergence

Even if the velocity vector $\dot{\bar{r}}$ asymptotically tracks the desired velocity $\dot{\bar{r}}_d = h(\bar{r})$ as above, it is not obvious that the vehicle position converges to the desired attractor, given by $V_F(\bar{r}) = 0$ [or $V_W(\bar{r}) = 0$]. The system can be recognized as a cascade of an asymptotically stable autonomous system (31) driving the vector field system via the connection $\bar{e} = \dot{\bar{r}} - h(\bar{r})$, where Eq. (31) can be written in the form $\dot{\bar{e}} = -P(\bar{e})$. As shown by an example [29], convergence of $\bar{e}$ to zero does not generally imply that the system $\dot{\bar{r}} = h(\bar{r}) + \bar{e}$ has a convergent (or even bounded) $\bar{r}$ when $\dot{\bar{r}} = h(\bar{r})$ is globally asymptotically stable. For stability of equilibria (as opposed to more general attractors as studied here), [8] shows that linear boundedness in $\bar{r}$ of the coupling term $\bar{e}$ is enough to give

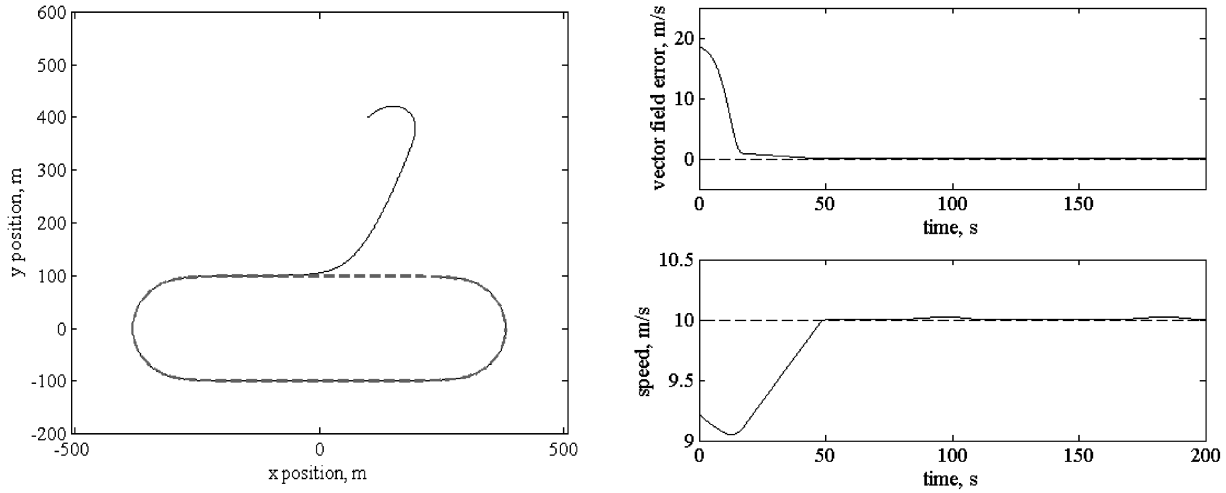

Fig. 8 Tracking simulation using the control law (34), with $m = 3$, $l = 0.03$, and $v = 10$ m/s.

convergent-input-convergent-state stability. In two dimensions, more general attractor convergence can be shown using the Poincaré–Bendixson theorem [24]. In three dimensions, this can be investigated using the vector field Lyapunov function $V_F(\bar{r})$ [or $V_W(\bar{r}) = 0$], but with $\bar{r}$ resulting from the control law (31). Using the case of $V_F(\bar{r})$, this produces

$$\dot{V}_F(\bar{r}) = \frac{\partial V_F}{\partial \bar{r}}\dot{\bar{r}} = \frac{\partial V_F}{\partial \bar{r}}\left((\dot{\bar{r}} - h(\bar{r})) - \left[\frac{\partial V_F}{\partial \bar{r}}\Gamma(\bar{r})\right]^T\right)$$
$$\leq \left|\frac{\partial V_F}{\partial \bar{r}}\right|\left(|\dot{\bar{r}} - h(\bar{r})| - \lambda_{\min}\{\Gamma(\bar{r})\}\left|\frac{\partial V_F}{\partial \bar{r}}\right|\right) \tag{39}$$

using, for example, Eq. (3) for $h(\bar{r})$, the Rayleigh property for symmetric matrices, and the Cauchy–Schwartz inequality. Then Eq. (38) is negative on any time interval L_i where

$$\lambda_{\min}\{\Gamma(\bar{r})\}\left|\frac{\partial V_F}{\partial \bar{r}}\right| > 2|\dot{\bar{r}} - h(\bar{r})| \tag{40}$$

in which case $V_F(\bar{r})$ is decreasing. On any other time interval J_i

$$\lambda_{\min}(\Gamma(\bar{r}))\left|\frac{\partial \bar{V}_F}{\partial \bar{r}}\right| \leq 2|\dot{\bar{r}} - h(\bar{r})| \tag{41}$$

Since $(\partial V_F/\partial \bar{r})\Gamma(\bar{r}) \to 0$ implies $V_F(\bar{r}) \to 0$ by assumption A3 and the uniformly positive definite condition on $\Gamma(\bar{r})$, then for any $\varepsilon > 0$ there exists a $\delta > 0$ such that $\lambda_{\min}\{\Gamma(\bar{r})\}|\partial V_F/\partial \bar{r}| < \delta$ implies that $V_F(\bar{r}) < \varepsilon$. Since $\dot{\bar{r}} - h(\bar{r}) \to 0$ from Theorem 2 and a suitable choice of the control law P (as shown in the previous examples), there exits a t_1 such that $|\dot{\bar{r}} - h(\bar{r})| < \delta/2$ for all $t > t_1$. If there exist any J_i intervals where $t > t_1$, we have $V_F(\bar{r}) < \varepsilon$ on those intervals, and for any of the L_i intervals where $t > t_1$, we have $V_F(\bar{r})$ monotone decreasing, hence $V_F(\bar{r}) < \varepsilon$ after any such J_i interval. Since $\varepsilon > 0$ was arbitrary, $V_F(\bar{r}) \to 0$. If for any t_1, no such J_i intervals exist, then a single L_i interval exists for all $t > t_1$ where

$$\dot{V}_F(\bar{r}) < -\frac{1}{2}\left|\frac{\partial V_F}{\partial \bar{r}}\right|\lambda_{\min}\{\Gamma(\bar{r})\}\left|\frac{\partial V_F}{\partial \bar{r}}\right|$$

By the arguments in Theorem 1, $V_F(\bar{r}) \to 0$. Thus, asymptotic tracking of the vector field $\dot{\bar{r}} - h(\bar{r}) \to 0$ implies asymptotic convergence to the desired attractor $V_F(\bar{r}) = 0$.

Figure 8 shows a simulation of the control law (34) applied to the racetrack vector field, beginning with an initial velocity approximately in the opposite direction of the vector field. Low gains (l, m) are able to produce accurate tracking of the racetrack pattern due to the feedforward of the known vector field acceleration in Eq. (31). These gains also limit turn rates and speed variation and can be set to correspond to vehicle maneuvering capabilities.

V. Conclusions

By considering contraction and circulation terms in the vector field separately, the Lyapunov approach produces vector fields that are globally attractive to a desired closed path and have desirable nonzero velocities for feasible UA flight. This simple, robust behavior enables decisions to be moved to higher levels in the control hierarchy and simplifies the construction of more complex behavior by using the vector field as a motion primitive. The example of switching loiter circle vector fields to follow arbitrary waypoint sequences illustrates this building block approach to UA guidance using well-behaved primitives.

Separation of the guidance and control portions of UA flight control provides the flexibility to design guidance vector fields independently from the control laws used to track the vector field. This enables a simplification in the analysis which permits a more general approach to constructing vector fields that have provable stability properties. The general framework, in turn, enables variations that increase the range of applications that the vector field approach can serve, for example, by varying the shape, size, or location of the global attractor.

Tracking of the vector field was shown to be globally stable using several different control laws, one that corresponds with the well-known planar kinematic model of flight at constant altitude, and others that enable more general 3-D attractors to be followed. Because of the simplicity of the vector fields and tracking laws, vector field guidance and on-board planning using vector fields is compatible with low-capability avionics processors found in low cost and micro UAs.

Acknowledgment

Research support for this work was provided by the National Science Foundation through the Information Technology Research Program Grant No. 042574744. This support is gratefully acknowledged.

References

[1] Park, S., Deyst, J., and How, J., "A New Nonlinear Guidance Logic for Trajectory Tracking," *Proceedings of the AIAA Guidance, Navigation, and Control Conference*, AIAA, Reston, VA, Aug. 2004, pp. 941–956.

[2] Osborne, J., and Rysdyk, R., "Waypoint Guidance for Small UAVs in Wind," *Proceedings of Infotech@Aerospace*, AIAA, Reston, VA, 2005, pp. 26–29.

[3] Galzi, D., and Shtessel, Y., "UAV Formations Control Using High Order Sliding Modes," AIAA Paper 2005-6367, 2005.

[4] Dogan, A., "Probabilistic Path Planning for UAVs," AIAA Paper 2003-6552, 2003.

[5] Parunak, H., Purcell, M., and O'Connell, R., "Digital Pheromones for Autonomous Coordination of Swarming UAVs," AIAA Paper 2002-3446, May, 2002.

[6] Paley, D., Leonard, N., and Sepulchre, R., "Oscillator Models and Collective Motion Splay State Stabilization of Self-Propelled Particles," *Proceedings of the IEEE Conference on Decision and Control, and the European Control Conference*, IEEE, Piscataway, NJ, Dec. 2005, pp. 3935–3940.
[7] Phillips, W. F., *Mechanics of Flight*, Wiley, New York, 2004, Chap. 7.
[8] Jankovic, M., Sepulchre, R., and Kokotovic, P., "Constructive Lyapunov Stabilization of Nonlinear Cascade Systems," *IEEE Transactions on Automatic Control*, Vol. 41, No. 12, Dec. 1996, pp. 1723–1735.
doi:10.1109/9.545712
[9] Michałek, M., and Kozłowski, K., "Trajectory Tracking for a Threecycle Mobile Robot: The Vector Field Orientation Approach," *Proceedings of the IEEE Conference on Decision and Control, and the European Control Conference*, IEEE, Piscataway, NJ, Dec., 2005, pp. 1119–1124.
[10] Niculescu, N., "Lateral Track Control Law for Aerosonde UAV," AIAA Paper 2001-16, Jan. 2001.
[11] Frew, E. W., "Comparison of Lateral Controllers for Following Linear Structures Using Computer Vision," *Proceedings of the American Control Conference*, IEEE, Piscataway, NJ, June 2006, pp. 2154–2159.
[12] Nelson, D. R., Barber, D. B., McLain, T. W., and Beard, R. W., "Vector Field Path Following for Miniature Air Vehicles," *IEEE Transactions on Robotics and Automation*, Vol. 23, No. 3, June 2007, pp. 519–529.
[13] Rysdyk, R., "Unmanned Aerial Vehicle Path Following for Target Observation in Wind," *Journal of Guidance, Control, and Dynamics*, Vol. 29, No. 5, 2006, pp. 1092–1100.
doi:10.2514/1.19101
[14] Rysdyk, R., Lum, C., and Vagners, J., "Autonomous Orbit Coordination for Two Unmanned Aerial Vehicles," AIAA Paper 2005-6362, Aug. 2005.
[15] Frew. E. W., Lawrence, D. A., and Morris, S., "Cooperative Standoff Tracking of Moving Targets Using Lyapunov Guidance Vector Fields," *Journal of Guidance, Control, and Dynamics*, Vol. 31, No. 2, March–April 2008, pp. 290–306.
doi:10.2514/1.30507
[16] Lawrence, D., "Lyapunov Vector Fields for UAV Flock Coordination," AIAA Paper 2003-6575, 2003.
[17] Griffiths, S. R., "Vector Field Approach for Curved Path Following for Miniature Aerial Vehicles," AIAA Paper 2006-6467, Aug. 2006.
[18] Waydo, S., and Murray, R. M., "Vehicle Motion Planning Using Stream Functions," *Proceedings of the IEEE International Conference on Robotics and Automation*, IEEE, Piscataway, NJ, Sept. 2003, pp. 2484–2491.
[19] Justh, E., and Krishnaprasad, P., "Steering Laws and Continuum Models for Planar Formations," *Proceedings of the IEEE International Conference on Decision and Control*, IEEE, Piscataway, NJ, Dec. 2003, pp. 3609–3614.
[20] Frew, E., and Lawrence, D., "Cooperative Stand-Off Tracking of Moving Targets by a Team of Autonomous Aircraft," AIAA Paper 2005-6363, Aug. 2005.
[21] Pisano, W. J., and Lawrence, D. A., "Concentration Gradient and Information Energy for Decentralized UAV Control," AIAA Paper 2006-6459, Aug. 2006.
[22] Frew, E. W., "Cooperative Stand-Off Tracking of Uncertain Moving Targets Using Active Robot Networks," *Proceedings of the IEEE International Conference on Robotics and Automation*, IEEE, Piscataway, NJ, April 2007, pp. 3277–3282.
[23] Guckenheimer, J., and Holmes, P., *Nonlinear Oscillations, Dynamical Systems, and Bifurcations of Vector Fields*, Springer–Verlag, Berlin, 1983, pp. 86–91.
[24] Khalil, H., *Nonlinear Systems*, 3rd ed., Prentice–Hall, Upper Saddle River, NJ, 2001, p. 323.
[25] Beard, R., Kingston, D., Quigley, M., Snyder, D., Christiansen, R., Johnson, W., McLain, T., and Goodrich, M., "Autonomous Vehicle Technologies for Small Fixed-Wing UAVs," *Journal of Aerospace Computing, Information, and Communication*, Vol. 2, Jan. 2005, pp. 92–108.
doi:10.2514/1.8371
[26] Grundel, D., and Jeffcoat, D., "Formulation and Solution of the Target Visitation Problem," Paper 2004-6212, 2004.
[27] McConnell, A. J., *Applications of Tensor Analysis*, Dover, New York, 1957, pp. 20–22.
[28] Desoer, C. A., and Vidyasagar, M., *Feedback Systems: Input-Output Properties*, Academic Press, New York, 1975, p. 252.
[29] Sontag, E. D., "Remarks on Stabilization and Input-to-State Stability," *Proceedings of the IEEE Conference on Decision and Control*, IEEE, Piscataway, NJ, Dec. 1989, pp. 1376–1378.